

Melt in Antarctica derived from Soil Moisture and Ocean Salinity (SMOS) observations at L band

Marion Leduc-Leballeur, Ghislain Picard, Giovanni Macelloni, Arnaud Mialon, Yann H. Kerr

▶ **To cite this version:**

Marion Leduc-Leballeur, Ghislain Picard, Giovanni Macelloni, Arnaud Mialon, Yann H. Kerr. Melt in Antarctica derived from Soil Moisture and Ocean Salinity (SMOS) observations at L band. The Cryosphere, 2020, 14, pp.539-548. 10.5194/tc-14-539-2020 . insu-03668289

HAL Id: insu-03668289
https://insu.hal.science/insu-03668289

Submitted on 16 May 2022

HAL is a multi-disciplinary open access archive for the deposit and dissemination of scientific research documents, whether they are published or not. The documents may come from teaching and research institutions in France or abroad, or from public or private research centers.

L'archive ouverte pluridisciplinaire **HAL**, est destinée au dépôt et à la diffusion de documents scientifiques de niveau recherche, publiés ou non, émanant des établissements d'enseignement et de recherche français ou étrangers, des laboratoires publics ou privés.



Distributed under a Creative Commons Attribution 4.0 International License

The Cryosphere, 14, 539–548, 2020
https://doi.org/10.5194/tc-14-539-2020
© Author(s) 2020. This work is distributed under
the Creative Commons Attribution 4.0 License.

The Cryosphere Open Access EGU

Melt in Antarctica derived from Soil Moisture and Ocean Salinity (SMOS) observations at L band

Marion Leduc-Leballeur[1,2], Ghislain Picard[2], Giovanni Macelloni[1], Arnaud Mialon[3], and Yann H. Kerr[3]

[1]Institute of Applied Physics "Nello Carrara", National Research Council, 50019 Sesto Fiorentino, Italy
[2]UGA, CNRS, Institut des Géosciences de l'Environnement (IGE), UMR 5001, 38041 Grenoble, France
[3]CESBIO, CNES–CNRS–IRD–UPS, University of Toulouse, 31401 Toulouse CEDEX 09, France

Correspondence: Marion Leduc-Leballeur (m.leduc@ifac.cnr.it)

Received: 20 August 2019 – Discussion started: 20 September 2019
Revised: 15 December 2019 – Accepted: 9 January 2020 – Published: 11 February 2020

Abstract. Melt occurrence in Antarctica is derived from L-band observations from the Soil Moisture and Ocean Salinity (SMOS) satellite between the austral summer 2010–2011 and 2017–2018. The detection algorithm is adapted from a threshold method previously developed for 19 GHz passive microwave measurements from the special sensor microwave imager (SSM/I) and special sensor microwave imager sounder (SSMIS). The comparison of daily melt occurrence retrieved from 1.4 and 19 GHz observations shows an overall close agreement, but a lag of few days is usually observed by SMOS at the beginning of the melt season. To understand the difference, a theoretical analysis is performed using a microwave emission radiative transfer model. It shows that the sensitivity of 1.4 GHz signal to liquid water is significantly weaker than at 19 GHz if the water is only present in the uppermost tens of centimetres of the snowpack. Conversely, 1.4 GHz measurements are sensitive to water when spread over at least 1 m and when present in depths up to hundreds of metres. This is explained by the large penetration depth in dry snow and by the long wavelength (21 cm). We conclude that SMOS and higher-frequency radiometers provide interesting complementary information on melt occurrence and on the location of the water in the snowpack.

1 Introduction

Melt occurs in coastal Antarctica and on ice shelves during the austral summer. Its duration and extent are useful climate indicators due to their connection to surface temperature and surface energy budget (e.g. Liu et al., 2006; Picard et al., 2007). Moreover, intense melting has been identified as a precursor of some major ice shelf collapses (Scambos et al., 2000). Thus, monitoring of the melt season contributes to characterizing the seasonal and interannual climatic variations in Antarctica and is important for assessing the future stability of the ice sheet (Golledge et al., 2015).

Remote sensing offers a particularly relevant means to obtain information over the entire Antarctic continent and over long-term periods, given the very rare in situ measurements related to melt or liquid water (Jakobs et al., 2019). Microwave frequencies have been widely used to detect melt in polar regions, exploiting the marked variation in the signal due to the high absorption of microwaves by water relative to that of dry snow. Various detection algorithms have been developed for active sensors (e.g. Nghiem et al., 2001, 2005; Ashcraft and Long, 2006; Kunz and Long, 2006; Hall et al., 2009; Trusel et al., 2012; Zheng et al., 2019) and passive sensors (e.g. Mote et al., 1993; Ridley, 1993; Zwally and Fiegles, 1994; Abdalati and Steffen, 1997; Torinesi et al., 2003; Liu et al., 2005, 2006; Tedesco, 2007; Tedesco et al., 2007) and applied to the Greenland and Antarctic ice sheets.

In the case of radiometer measurements, studies have mainly used 19 and 37 GHz frequencies available since 1979 from several satellite sensors such as the scanning multichannel microwave radiometer (SMMR) on the Nimbus 7 satellite or the special sensor microwave imager (SSM/I) and special sensor microwave imager sounder (SSMIS) from the Defense Meteorological Satellite Program (DMSP) satellites. Since 2009, the Soil Moisture and Ocean Salinity (SMOS) satellite has provided radiometric observations at the L band,

a frequency capable of penetrating much deeper into the ice sheets, on the order of several hundred metres at 1.4 GHz (Passalacqua et al., 2018) compared to only a few metres for the higher frequencies (Surdyk, 2002). This suggests that L-band observations could offer new information on melt.

The aim of this study is to retrieve melt in Antarctica from daily SMOS observations and to investigate the similarities and differences with melt detected at 19 GHz. Section 2 introduces the datasets. Section 3 describes the method for detecting melt, and Sect. 4 compares the daily melt occurrence obtained with 1.4 and 19 GHz observations. Section 5 presents a modelling study to assess the liquid water sensitivity of brightness temperature (T_B) at 1.4 GHz and to discuss the differences with 19 GHz.

2 Datasets

2.1 SMOS observations

The SMOS mission was developed by the European Space Agency (ESA) in collaboration with the Centre National d'Études Spatiales (CNES) in France and the Centro para el Desarrollo Tecnológico Industrial (CDTI) in Spain. This satellite is operated by CNES and ESA and carries on board a L-band interferometric radiometer operating at 1.4 GHz (21 cm) with an averaged ground resolution of 43 km (Kerr et al., 2010). The radiometer provides multi-angular fully polarized T_B (Kerr et al., 2001).

The SMOS Level 3 product delivers multi-angular T_B at the top of the atmosphere in the antenna polarization reference frame (Al Bitar et al., 2017). The product is georeferenced on the Equal-Area Scalable Earth version 2.0 grid (EASE-Grid 2; Brodzik et al., 2012), with an oversampled resolution of about 628 km^2, which is distorted in the polar regions (around 100 km × 6 km as latitude × longitude). It comprises the daily average and incident-angle average, with angle bins every 5° from 0 to 65°. T_B values at vertical (V) and horizontal (H) polarizations for the 50–55° average range of incidence angle are used here. They come from the RE04 reprocessed version between April 2010 and April 2015 and from the operational version between May 2015 to March 2018, both distributed by CATDS (Centre Aval de Traitement des Données SMOS; https://www.catds.fr/, last access: 9 February 2020).

The gaps shorter than 3 d in the SMOS time series are filled by a linear interpolation. Longer gaps result in missing values in the product. If more than 60 d are missing over a year, the grid point is ignored for that year (about 7 % of pixel every year, mainly south of 83° S).

The land–ocean mask used comes from the Land-Ocean-Coastline-Ice classification associated with the EASE-Grid 2.0 map projections and derived from the MODIS land cover product by Brodzik and Knowles (2011) (available at: https://nsidc.org/data/nsidc-0609, last access: 9 February 2020).

2.2 Observations at 19 GHz and daily surface melting

Satellite observations at 19 GHz were acquired by the SSM/I and Special SSMIS, processed by the National Snow and Ice Data Center (NSIDC; Maslanik and Stroeve, 2004).

Daily T_B observations at H polarization are processed according to Picard and Fily (2006) to derive daily surface melt from 1979 to 2018 (available at: http://gp.snow-physics.science/melting last access: 9 February 2020). This dataset provides daily melt status, i.e. presence or absence of liquid water, for every grid point on the southern stereographic polar grid with a grid spacing of 25 km^2. The effective resolution of the product is coarser, of the order of 40 km, close to that provided by SMOS.

To compare SMOS and SSMIS datasets, the SSMIS observations and products are collocated within the SMOS grid using the nearest neighbour method. If the nearest neighbour is not flagged as "land" in the SSMIS grid, the pixel was removed from the analysis to avoid the error of comparison between the two frequencies. In this way, about 50 pixels are excluded, which does not affect the statistical significance of the comparison results.

3 Melting detection method

The algorithm for detecting melt occurrence from the 1.4 GHz observations is inspired by the work at 19 GHz of Torinesi et al. (2003), itself based on Zwally and Fiegles (1994). The algorithm determines an optimal threshold for every year in every pixel and considers that any daily $T_B H$ over this threshold indicates melting occurrence. T_B is measured at large observation angles (above 50°). In this configuration, the H polarization is favoured because the emissivity of dry firn is usually significantly lower at H than at V polarization, while the emissivity of wet firn is always close to 1 at both polarizations. It results in the increase in T_B from dry to wet snow being more significant at H polarization and easier to detect.

The algorithm uses an adaptive threshold T in each grid point and for each year given by $T = M + a\sigma$, with M being the time average and σ the standard deviation of T_B when snow is dry. According to the analysis of daily air surface temperature, Torinesi et al. (2003) found a suitable value of $a = 3$ so that most melting events correspond to daily maximum temperatures above −5 °C. This value is also typical for outlier detection (e.g. von Storch and Zwiers, 2001).

To solve the circular problem of computing M and σ for non-melting days in order to detect melting days, the initial step consists of calculating M in each grid point on a fixed period of 1 year – from 1 April to 31 March – and in setting $a\sigma$ to a first-guess fixed value. Previous studies for 19 GHz

used $a\sigma = 30$ K. However, we found it unsuitable at 1.4 GHz because of the weaker sensitivity to liquid water (Sect. 5). We instead propose a lower first-guess value of $a\sigma = 15$ K.

With these assumptions, a first-guess melt time series is detected, and new estimates of M and σ are computed by removing melting days from the T_B series, still limiting the period from 1 April and 31 March. Melt is then detected once again using the updated threshold. The process is iterated three times to ensure stable estimates. The algorithm returns a binary indicator for each day and each grid point, 0 for the absence and 1 for the presence of liquid water.

This algorithm needs further correction for some false alarms found on the Antarctic Plateau, where melt is known to never occur. These alarms are likely due to variations in $T_B H$ of the order of several kelvin that were reported by Brucker et al. (2014) and Leduc-Leballeur et al. (2017) and are explained to result from the snow metamorphism and surface hoar removal by wind storms. Noting that these changes do not impact $T_B V$, although melt does, we consider here that the areas with low annual standard deviation of $T_B V$ are not subject to melt. We estimated a threshold standard deviation of 2.8 K based on the fact that it excludes 95 % of grid points with surface elevation higher than 1500 m. Thus, as a final step of the algorithm, the grid points with a $T_B V$ annual standard deviation lower than this threshold are masked out for that year.

4 Comparison with 19 GHz

Figure 1 shows two examples of two consecutive melt seasons in the Amery area (69.97° S, 73.53° E) and the Antarctic Peninsula (66.81° S, 64.19° W). For each event, melt is detected several days earlier at 19 GHz compared to 1.4 GHz. For instance, in 11 December 2013 in the Amery time series, a short melting event lasting for 6 d is missed at 1.4 GHz, while it is well detected at 19 GHz. This suggests that this event was weak and only affected the superficial part of the snowpack. On the other hand, the short melting event during March 2015 in the peninsula time series is detected by both frequencies, suggesting intense melt with percolation in a large upper part of the snowpack.

The beginning of the melt season detected usually largely differs between both frequencies, as illustrated in Fig. 2. On average, the first melting day can be detected as early as September at 19 GHz, while it is rare to detect melt earlier than December at 1.4 GHz. For the pixel where melt is detected by both frequencies in a given year, the 19 GHz detection precedes the 1.4 GHz detection by 1–5 d for 28 % of the pixels and by 6–15 d for 26 % of them. This lag is also observed for the end of the season, with a persistence of the melt detected at 1.4 GHz until nearly April.

Figure 2 also highlights that the melt extent detected at 19 GHz is 3 to 6 times as large as at 1.4 GHz, depending on the years. The standard deviation maximum is reached in January at 250 000 and 110 000 km^2 for 19 and 1.4 GHz, respectively. Spatial variations are illustrated by Fig. 3, which shows the annual mean duration of the melt season between April 2010 and March 2018 detected at both frequencies. Melting is concentrated on the coast, with a maximum in the Antarctic Peninsula, as previously reported for 19 GHz (Tedesco, 2009; Kuipers Munneke et al., 2012; Datta et al., 2018, 2019; Scott et al., 2019). The largest differences are observed in the Filchner and Ross ice shelves, where melt is detected to occur on a few days every year at 19 GHz but is insufficient to be detected at 1.4 GHz. The difference is certainly explained by the difference of sensitivity. Indeed, as these ice shelves only experience limited melt, the liquid water is likely concentrated in the uppermost few centimetres of the snowpack.

Figures 3 and 4 highlight that 19 GHz is more effective for detecting short melting duration than 1.4 GHz. Indeed, more than 55 % of the pixels where melt occurs remain wet for less than 10 d in a year, according to 19 GHz observations, and about 20 % remain wet between 11 and 20 d. At 1.4 GHz, the duration of the melt season is usually longer. In only 20 % of the pixels subject to melt, the season is 1–10 d; it is 11–40 d in 55 % of the pixels. This hints at the fact that SMOS is only sensitive to long and intense melt seasons.

However, it also happens that some melting days are detected with the 1.4 GHz observations but not with the 19 GHz observations. This case is illustrated with the example of the Antarctic Peninsula provided in Fig. 5 for the three summer seasons from 2013 to 2016. This area is known to be subjected each year to a long melt season, but high interannual variability is observed. Zheng et al. (2019) studied the Antarctic Peninsula with a satellite radiometer and scatterometer as well as a climate model. They found that over the period 2010–2017 the lowest wet-snow extent is observed during the 2013–2014 summer season, whereas the largest is observed during 2015–2016. These two particular events are also retrieved by SMOS and SSMIS during this period.

Figure 5g, h and i show the number of days detected as melting at 1.4 GHz but being dry at 19 GHz. In 2013–2014, 2.6 d on average are only detected as melting by SMOS over a surface of 35 625 km^2 (57 pixels). In 2015–2016, 12.3 d on average are only detected as melting by SMOS over a surface of 83 125 km^2 (133 pixels), which is 57 % and 24 % larger than in 2013–2014 and 2014–2015, respectively. As 2015–2016 is known to have been subjected to an intensive melting event in the Antarctic Peninsula due to a strong El Niño event (Nicolas et al., 2017), this could suggest that 1.4 GHz provides additional information to 19 GHz in the case of intense melting events. In this way, Wiesenekker et al. (2018) showed that a stronger-than-normal foehn wind, which is a hot, dry wind on the downwind side of a mountain range, happens over the peninsula in 2015–2016. This generates an increase in melt near the foot of the Antarctic Peninsula mountains. This area matches the pixels where 1.4 GHz observations detected more than 20 d not detected by 19 GHz

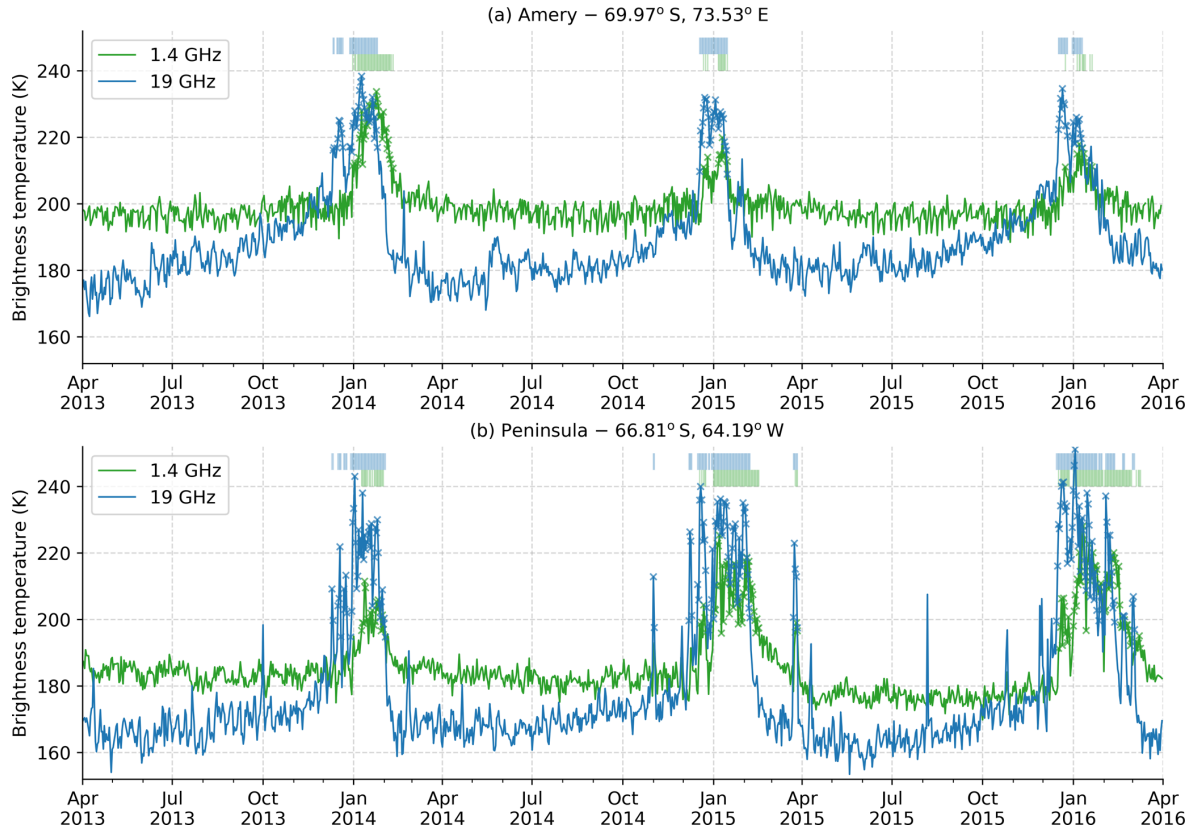


Figure 1. Brightness temperature at H polarization (K) at 1.4 GHz (green) and 19 GHz (blue) from April 2013 to March 2016 at **(a)** the Amery area and **(b)** the Antarctic Peninsula. The melting days detected by each frequency are depicted by crosses on the time series and recalled by pale lines above.

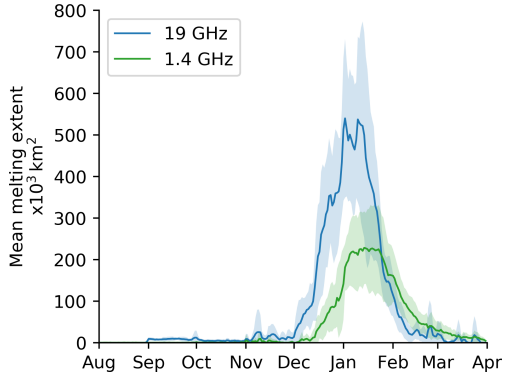


Figure 2. Daily mean melting extent from April 2010 to March 2018 detected with observations at 1.4 GHz (green) and at 19 GHz (blue). Standard deviation is in pale area.

(Fig. 5). Moreover, Datta et al. (2019) also found that high melt occurrence induced by foehn wind is observed in 2015–2016, and they highlighted that this foehn wind increases the meltwater percolation by up 2 m in depth along the mountains. This suggests that SMOS observations could provide information about a part of snowpack in depth which is not reached by SSMIS observations.

Figure 6 maps, for the whole continent, the mean number of melting days detected at 1.4 GHz without concurrent detection at 19 GHz during summer season over our dataset. It shows that the geographical distribution is related to the total number of melt events (Fig. 3), meaning that all the areas are concerned by the differential detection at both frequencies. On average, 10 ± 8 d are detected only by SMOS. Moreover, over a total of about 117 000 melting days, taking all pixels and summer seasons together that were detected at 1.4 GHz, 28 % are not concurrently detected at 19 GHz. These melting days happen on 1 February ± 23 d on average, i.e. at the end of summer season. Conversely, over 225 000 melting days are detected by 19 GHz during the same period, and 66 % are not concurrently detected at 1.4 GHz.

5 Sensitivity to liquid water content

The sensitivity to liquid water at 1.4 GHz is investigated in order to understand the signal variations observed in Antarctica and to investigate the observed differences with the 19 GHz melt detection.

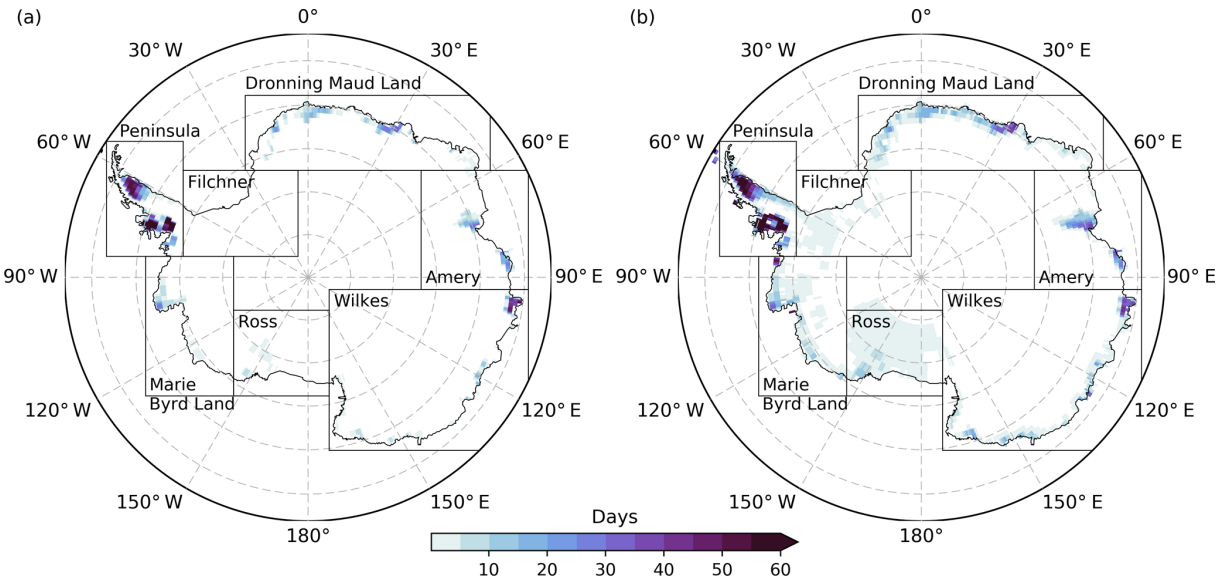


Figure 3. Annual mean of melting duration (days) from April 2010 to March 2018 detected with observations **(a)** at 1.4 GHz (SMOS) and **(b)** at 19 GHz (SSMIS). Seven regions are outlined.

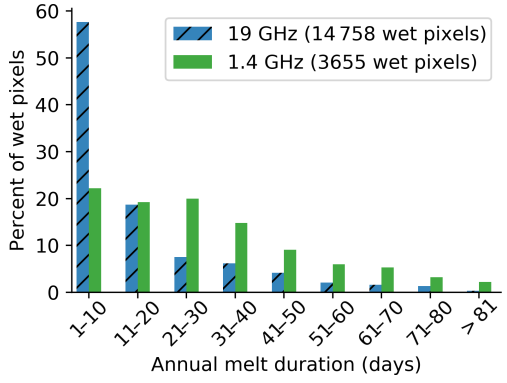


Figure 4. Annual melting duration distribution of wet pixels detected with 1.4 GHz (solid green) and 19 GHz (hatched blue) over the whole continent of Antarctica for each summer season from 2010 to 2018.

5.1 Microwave emission modelling

T_B is simulated with the multi-layered dense-medium radiative theory model (DMRT-ML; Picard et al., 2013), available at: http://gp.snow-physics.science/dmrtml (last access: 9 February 2020). This model is based on the radiative transfer theory (Tsang and Kong, 2001). The snowpack is represented by a stack of snow horizontal layers defined by their thickness, temperature, density, grain size and liquid water content (LWC). Simulations are performed at 1.4 and 19 GHz, with an incidence angle of 55°.

Synthetic snowpack is assumed to run simulations. It has a total thickness of 1000 m and is divided into layers of 5 cm from the surface to 500 and 50 m below. The temperature is 273 K from the surface to 5 m in depth, then constant at 263 K up to 500 m depth and, finally, linearly increases to reach 273 K at the bottom. Density linearly increases from 300 kg m^{-3} at the surface to 917 kg m^{-3} at 100 m in depth and is constant below (Leduc-Leballeur et al., 2015). Grain size is constant, at 1 mm. Picard et al. (2013) showed that grain size has an effect on the sensitivity to LWC at 19 GHz. Nevertheless, it is not expected at 1.4 GHz because the wavelength is much larger than grain size and scattering by grains can be neglected (Mätzler, 1987).

5.2 Effect of snow density vertical variability

By modelling L-band emission at Dome C on the Antarctic Plateau, Leduc-Leballeur et al. (2015) highlighted that layering must be considered to obtain reliable T_B estimation. To assess if this is also the case for wet snow, the simulations are performed with a smooth density profile and two density profiles with an added Gaussian noise of a standard deviation of 10 and 20 kg m^{-3}, respectively, between the surface and 300 m in depth. Figure 7 shows the DMRT-ML simulations at both 1.4 and 19 GHz as a function of LWC and for various thicknesses of wet snow.

For the dry snowpack (LWC = 0 kg m^{-2}), the layering significantly decreases $T_B H$ from 248.1 K for the smooth density profile to 231.8 and 196.9 K for the density profiles with a standard deviation of 10 and 20 kg m^{-3}, respectively. In the wet-snow condition, the layering effect becomes weaker as the LWC increases and is insignificant (< 4 K variations) for LWC larger than 1 kg m^{-2} or when water is spread over a large thickness. Thus, between dry and wet conditions, the $T_B H$ difference increases with the layering.

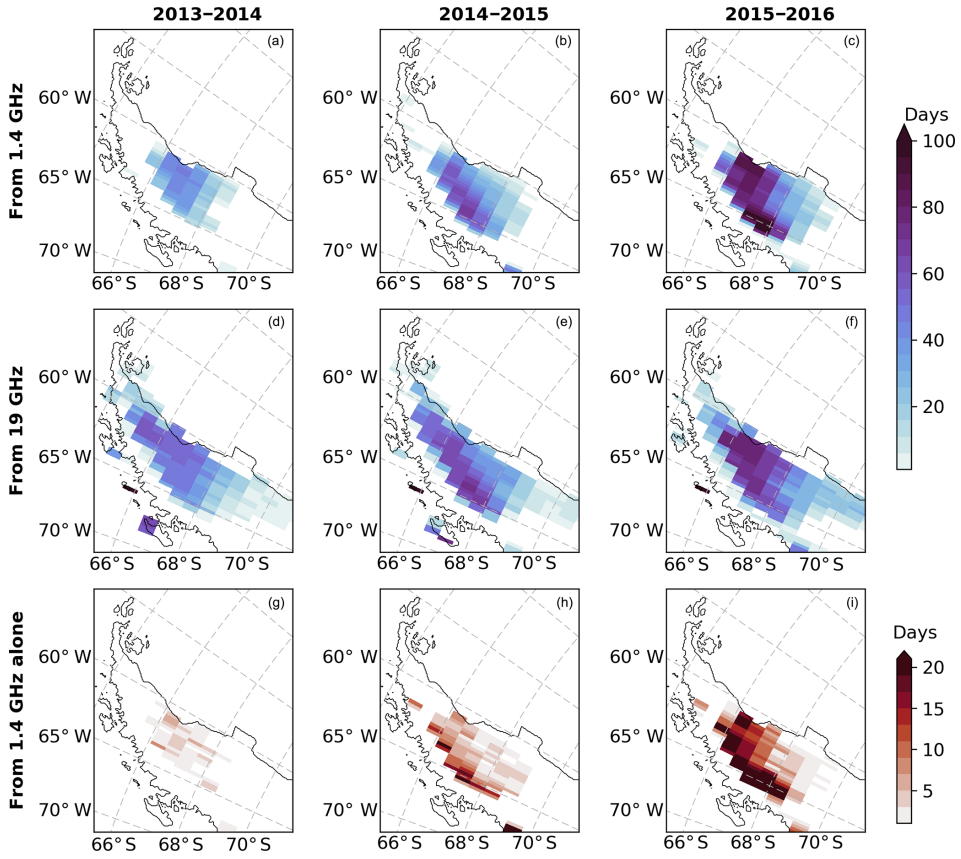


Figure 5. Annual melting duration (days) over the Antarctic Peninsula detected with observations **(a–c)** at 1.4 GHz and **(d–f)** at 19 GHz from 2013–2014 to 2015–2016. **(g–i)** Number of days detected as melting at 1.4 GHz but dry at 19 GHz.

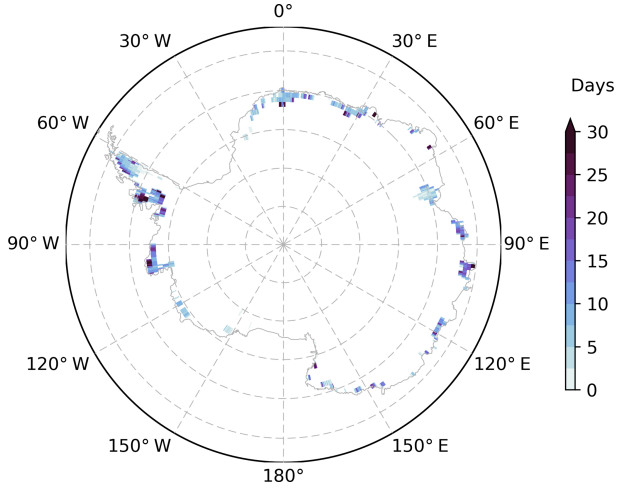


Figure 6. Mean melting days by summer season detected as melting at 1.4 GHz but dry at 19 GHz.

Figure 7d shows daily SMOS $T_B H$ from June to August – a period when snow is expected to always be dry – in 2010–2018. The histogram only includes pixels where melting has been detected at least once and where ice thickness is 1000 ± 50 m to match with the snowpack configuration used for simulations. The SMOS $T_B H$ average is 206.9 ± 8.9 K. This suggests that simulations with a density variability lower than 10 kg m^{-3} overestimate the dry $T_B H$ and thus underestimate the variations between dry and wet snow at 1.4 GHz. We thus now consider the case of a density variability of 20 kg m^{-3} only.

The simulations show that $T_B H$ at 1.4 GHz increases from dry to wet by 19 K when the wet-snow layer is 0.25 m and 53 K when it is 5 m (Fig. 7c). While in both cases, the change is high and detectable, this highlights not only the importance of the total column amount of liquid water but also that of the distribution at depth. Additionally, Fig. 7c shows that the maximum increase in $T_B H$ is reached for LWC of 0.75 and 0.15 kg m^{-2}, respectively, for the 0.25 and 5 m thick wet-snow layers. This means that the LWC sensitivity of 1.4 GHz $T_B H$ is weaker when liquid water is confined to the uppermost tens of centimetres of the snowpack. This is the rationale for choosing a lower first-guess $a\sigma$ for the detection algorithm at 1.4 GHz than at the higher frequencies (Sect. 3).

Additionally, Fig. 7c shows that regardless of the wet-layer thickness, $T_B H$ reaches a maximum at a certain LWC value, which decreases when the wet layer becomes thicker. Thus,

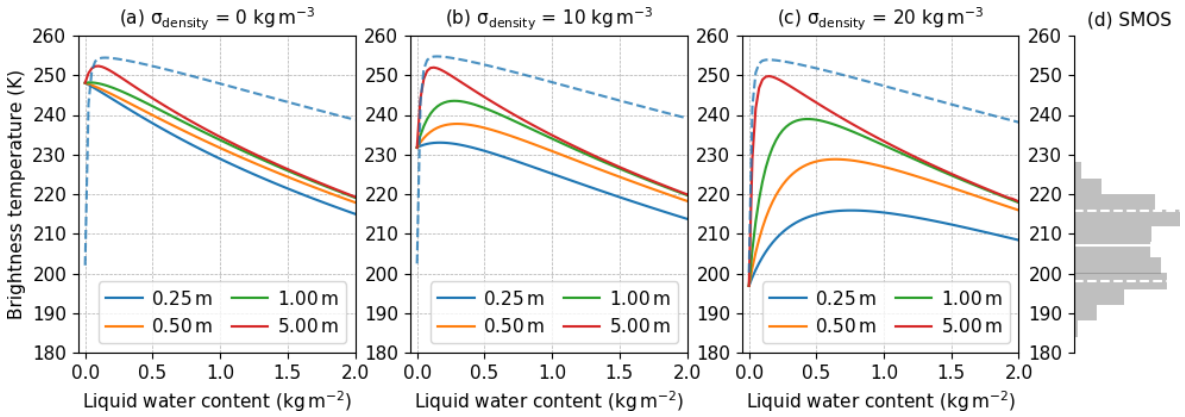


Figure 7. (a–c) DMRT-ML brightness temperature at H polarization (K) as a function of liquid water content for several wet-snow thicknesses in the upper snowpack (colours) at 1.4 GHz (solid lines) and 0.25 m of wet snow at 19 GHz (dashed line), with three density variabilities ($\sigma_{density}$). **(d)** Daily winter SMOS observations distribution (see text for details), with mean (white solid) and standard deviation (white dashed).

an increase in LWC is not detectable because of the T_B saturation. This jeopardizes the possibility of using microwave observations to estimate LWC values or even the wet-layer thickness.

By contrast, at 19 GHz, the density variability has no effect, and the $T_B H$ variations are mainly driven by LWC. A sharp increase of 54 K is observed, and the maximum is reached for LWC of 0.15 kg m^{-2}. The thickness of the wet-snow layer has no effect (not shown in Fig. 7c).

In conclusion, these simulations show that 19 GHz is more sensitive to liquid water than at 1.4 GHz and that other factors such as the vertical distribution of the water or the layering have a smaller influence. This indicates that detection of melt occurrence at the surface is more robust at 19 GHz.

5.3 Effect of the wet-snow depth

We explore here the situation when the wet-snow layer is buried under a layer of dry firn. This corresponds to the end of summer, when the snowpack freezes up from the surface, or on the ice shelves, where meltwater enters the crevasses and accumulates at depth. The simulations are performed with a wet-snow layer (0.2 kg m^{-2}), progressively moving down from the surface to 400 m in depth. The wet-layer thickness is 1 m at 1.4 GHz and 0.1 m at 19 GHz to moderate the sensitivity effect presented in the previous section. Results highlight that $T_B H$ is maximum when wet snow is at the surface for both frequencies and decreases within a few metres at 19 GHz and more gradually at 1.4 GHz (Fig. 8). $T_B H$ is still more than 10 K higher than in dry conditions when the wet layer is at 60 m in depth at 1.4 GHz. Deeper than 100 m, the difference between dry and wet $T_B H$ is lower than 3 K, i.e. lower than the noise level with SMOS.

At 19 GHz, the simulation shows a $T_B H$ variation of 2 K between dry and wet when the wet snow is at 5 m in depth. Thus, the sensitivity to liquid water is relatively quickly lost

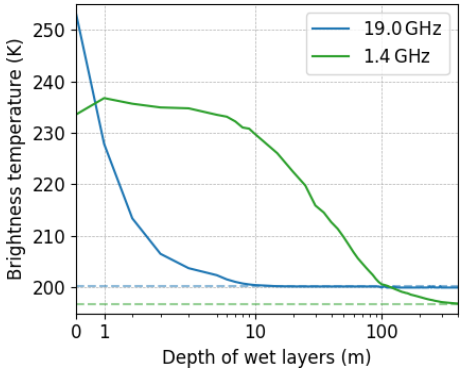


Figure 8. DMRT-ML brightness temperature at H polarization (K) for 55° of incidence angle as a function of the wet-snow-layer depth within the snowpack for a wet-layer thickness of 1 m at 1.4 GHz (green) and 0.1 m at 19 GHz (blue). Values for a dry snowpack are in dashed lines.

at this frequency if the water percolates deep into the firn. However, observations at 19 GHz should still be suitable for the detection of remnant liquid water at the end of the season and when the snowpack is continuous, i.e. without crevasse.

These results suggest that despite a lower sensitivity at 1.4 GHz, liquid water could be detected with SMOS up to several tens of metres at depth, and this is new information compared to that provided by the existing melt product derived from 19 GHz and higher-frequency observations. The difference observed between 19 and 1.4 GHz could be exploited to determine if the melt event was limited to the few first centimetres of snowpack or if water percolated over a sufficient thickness to be detected by SMOS.

6 Conclusions

The L-band brightness temperature (T_B) from the SMOS satellite has been explored to retrieve information about the melt season in Antarctica. Daily melt occurrence can be retrieved using previously developed algorithms for higher frequencies (Zwally and Fiegles, 1994; Torinesi et al., 2003) after a slight adaptation to account for the lower sensitivity at 1.4 GHz. The comparison of melt detected at 1.4 and 19 GHz (Picard and Fily, 2006) shows a lower rate of detection at 1.4 GHz. In particular, SMOS misses short, probably weak, events, which are in contrast perfectly detected by SSMIS.

A theoretical analysis has been performed using a snowpack emission radiative transfer model (DMRT-ML) in order to estimate the sensitivity of T_B at 1.4 and 19 GHz to liquid water content (LWC) and water distribution in the snowpack. As expected from previous studies, a clear increase in T_B happens when snow becomes wet. However, the simulations clearly demonstrate that 1.4 GHz is less sensitive than 19 GHz, especially when liquid water stays within the top centimetres of the snowpack. A thick wet layer (> about 0.5 m) is required to trigger a sharp and detectable T_B increase. Despite this limited sensitivity, the simulations show that 1.4 GHz is suitable to detect wet snow buried under a dry surface. For instance, an increase in T_B higher than 10 K with respect to a dry snowpack can be observed with liquid water at up to 60 m in depth, according to the simulation configuration.

An avenue is a combined use of both frequencies to determine if a melt event was limited to the surface of the snowpack or if it was intense enough to inject water at depths. However, further algorithmic work is needed to exploit this possibility of deep-water detection with SMOS.

Data availability. Data for daily occurrence of melt retrieved from SMOS are available at: https://www.catds.fr/Products/Available-products-from-CEC-SM/CryoSMOS-project (Picard and Leduc-Leballeur, 2020).

Author contributions. MLL, GP and GM led the study and performed the analysis. AM and YHK supported for using the SMOS observations. All authors contributed to the paper.

Competing interests. The authors declare that they have no conflict of interest.

Acknowledgements. The SMOS L3 product comes from the CATDS, managed for the CNES by IFREMER (Brest, France). We would also like to thank the editor and the two anonymous reviewers for their very helpful comments.

Financial support. This research has been supported by the ESA support through the CryoSMOS project (contract 4000112262/14/I-NB) and the French space agency (CNES) support through the SMOS TOSCA project.

Review statement. This paper was edited by Chris Derksen and reviewed by two anonymous referees.

References

Abdalati, W. and Steffen, K.: Snowmelt on the Greenland ice sheet as derived from passive microwave satellite data, J. Climate, 10, 165–175, https://doi.org/10.1175/1520-0442(1997)010<0165:SOTGIS>2.0.CO;2, 1997.

Al Bitar, A., Mialon, A., Kerr, Y. H., Cabot, F., Richaume, P., Jacquette, E., Quesney, A., Mahmoodi, A., Tarot, S., Parrens, M., Al-Yaari, A., Pellarin, T., Rodriguez-Fernandez, N., and Wigneron, J.-P.: The global SMOS Level 3 daily soil moisture and brightness temperature maps, Earth Syst. Sci. Data, 9, 293–315, https://doi.org/10.5194/essd-9-293-2017, 2017.

Ashcraft, I. S. and Long, D. G.: Comparison of methods for melt detection over Greenland using active and passive microwave measurements, Int. J. Remote Sens., 27, 2469–2488, https://doi.org/10.1080/01431160500534465, 2006.

Brodzik, M. J. and Knowles, K.: EASE-Grid 2.0 Land-Ocean-Coastline-Ice Masks Derived from Boston University MODIS/Terra Land Cover Data, Version 1, NASA National Snow and Ice Data Center Distributed Active Archive Center, Boulder, Colorado, USA, https://doi.org/10.5067/VY2JQZL9J8AQ, 2011.

Brodzik, M. J., Billingsley, B., Haran, T., Raup, B., and Savoie, M. H.: EASE-grid 2.0: Incremental but Significant Improvements for Earth-Gridded Data Sets, ISPRS Int. Geo-Inf., 1, 32–45, https://doi.org/10.3390/ijgi1010032, 2012.

Brucker, L., Dinnat, E. P., Picard, G., and Champollion, N.: Effect of snow surface metamorphism on Aquarius L-band radiometer observations at Dome C, Antarctica, IEEE T. Geosci. Remote, 52, 7408–7417, https://doi.org/10.1109/TGRS.2014.2312102, 2014.

Datta, R. T., Tedesco, M., Agosta, C., Fettweis, X., Kuipers Munneke, P., and van den Broeke, M. R.: Melting over the northeast Antarctic Peninsula (1999–2009): evaluation of a high-resolution regional climate model, The Cryosphere, 12, 2901–2922, https://doi.org/10.5194/tc-12-2901-2018, 2018.

Datta, R. T., Tedesco, M., Fettweis, X., Agosta, C., Lhermitte, S., Lenaerts, J., and Wever, N.: The Effect of Foehn-Induced Surface Melt on Firn Evolution Over the Northeast Antarctic Peninsula, Geophys. Res. Lett., 46, 3822–3831, https://doi.org/10.1029/2018GL080845, 2019.

Golledge, N. R., Kowalewski, D. E., Naish, T. R., Levy, R. H., Fogwill, C. J., and Gasson, E. G.: The multi-millennial Antarctic commitment to future sea-level rise, Nature, 526, 421–425, https://doi.org/10.1038/nature15706, 2015.

Hall, D. K., Nghiem, S. V., Schaaf, C. B., DiGirolamo, N. E., and Neumann, G.: Evaluation of surface and near-surface melt characteristics on the Greenland ice sheet using MODIS and QuikSCAT data, J. Geophys. Res.-Earth, 114 F04006, https://doi.org/10.1029/2009JF001287, 2009.

Jakobs, C. L., Reijmer, C. H., Kuipers Munneke, P., König-Langlo, G., and van den Broeke, M. R.: Quantifying the snowmelt–albedo feedback at Neumayer Station, East Antarctica, The Cryosphere, 13, 1473–1485, https://doi.org/10.5194/tc-13-1473-2019, 2019.

Kerr, Y. H., Waldteufel, P., Wigneron, J.-P., Martinuzzi, J., Font, J., and Berger, M.: Soil moisture retrieval from space: The Soil Moisture and Ocean Salinity (SMOS) mission, IEEE T. Geosci. Remote, 39, 1729–1735, https://doi.org/10.1109/36.942551, 2001.

Kerr, Y. H., Waldteufel, P., Wigneron, J.-P., Delwart, S., Cabot, F., Boutin, J., Escorihuela, M.-J., Font, J., Reul, N., Gruhier, C., Juglea, S. E., Drinkwater, M. R., Hahne, A., Martín-Neira, M., and Mecklenburg, S.: The SMOS mission: New tool for monitoring key elements ofthe global water cycle, Proc. IEEE, 98, 666–687, https://doi.org/10.1109/JPROC.2010.2043032, 2010.

Kuipers Munneke, P., Picard, G., van den Broeke, M. R., Lenaerts, J. T. M., and van Meijgaard, E.: Insignificant change in Antarctic snowmelt volume since 1979, Geophys. Res. Lett., 39, L01501, https://doi.org/10.1029/2011GL050207, 2012.

Kunz, L. B. and Long, D. G.: Melt Detection in Antarctic Ice Shelves Using Scatterometers and Microwave Radiometers, IEEE T. Geosci. Remote, 44, 2461–2469, https://doi.org/10.1109/TGRS.2006.874138, 2006.

Leduc-Leballeur, M., Picard, G., Mialon, A., Arnaud, L., Lefebvre, E., Possenti, P., and Kerr, Y.: Modeling L-band brightness temperature at Dome C in Antarctica and comparison with SMOS observations, IEEE T. Geosci. Remote, 53, 4022–4032, https://doi.org/10.1109/TGRS.2015.2388790, 2015.

Leduc-Leballeur, M., Picard, G., Macelloni, G., Arnaud, L., Brogioni, M., Mialon, A., and Kerr, Y.: Influence of snow surface properties on L-band brightness temperature at Dome C, Antarctica, Remote Sens. Environ., 199, 427–436, https://doi.org/10.1016/j.rse.2017.07.035, 2017.

Liu, H., Wang, L., and Jezek, K. C.: Wavelet-transform based edge detection approach to derivation of snowmelt onset, end and duration from satellite passive microwave measurements, Int. J. Remote Sens., 26, 4639–4660, 2005.

Liu, H., Wang, L., and Jezek, K. C.: Spatiotemporal variations of snowmelt in Antarctica derived from satellite scanning multichannel microwave radiometer and Special Sensor Microwave Imager data (1978–2004), J. Geophys. Res.-Earth, 111, F01003, https://doi.org/10.1029/2005JF000318, 2006.

Maslanik, J. and Stroeve, J.: DMSP SSM/I-SSMIS Daily Polar Gridded Brightness Temperatures, Version 4, NASA National Snow and Ice Data Center Distributed Active Archive Center, Boulder, Colorado, USA, https://doi.org/10.5067/AN9AI8EO7PX0, 2004, updated 2018.

Mätzler, C.: Applications of the interaction of microwaves with the natural snow cover, Remote Sens. Rev., 2, 259–387, https://doi.org/10.1080/02757258709532086, 1987.

Mote, T. L., Anderson, M. R., Kuivinen, K. C., and Rowe, C. M.: Passive microwave-derived spatial and temporal variations of summer melt on the Greenland ice sheet, Ann. Glaciol., 17, 233–238, https://doi.org/10.3189/S0260305500012891, 1993.

Nghiem, S., Steffen, K., Kwok, R., and Tsai, W. Y.: Detection of snowmelt regions on the Greenland ice sheet using diurnal backscatter change, J. Glaciol., 47, 539–547, https://doi.org/10.3189/172756501781831738, 2001.

Nghiem, S. V., Steffen, K., Neumann, G., and Huff, R.: Mapping of ice layer extent and snow accumulation in the percolation zone of the Greenland ice sheet, J. Geophys. Res.-Earth, 110, F02017, https://doi.org/10.1029/2004JF000234, 2005.

Nicolas, J. P., Vogelmann, A. M., Scott, R. C., Wilson, A. B., Cadeddu, M. P., Bromwich, D. H., Verlinde, J., Lubin, D., Russell, L. M., Jenkinson, C., Powers H. H., Ryczek M., Stone G., and Wille J. D.: January 2016 extensive summer melt in West Antarctica favoured by strong El Niño, Nat. Commun., 8, 15799, https://doi.org/10.1038/ncomms15799, 2017.

Passalacqua, O., Picard, G., Ritz, C., Leduc-Leballeur, M., Quiquet, A., Larue, F., and Macelloni, G.: Retrieval of the Absorption Coefficient of L-Band Radiation in Antarctica From SMOS Observations, Remote Sensing, 10, 1954, https://doi.org/10.3390/rs10121954, 2018.

Picard, G. and Fily, M.: Surface melting observations in Antarctica by microwave radiometers: Correcting 26-year time series from changes in acquisition hours, Remote Sens. Environ., 104, 325–336, https://doi.org/10.1016/j.rse.2006.05.010, 2006.

Picard, G. and Leduc-Leballeur, M.: Melting occurrence from SMOS observations, available at: https://www.catds.fr/Products/Available-products-from-CEC-SM/CryoSMOS-project, last access: 9 February 2020.

Picard, G., Fily, M., and Gallée, H.: Surface melting derived from microwave radiometers: a climatic indicator in Antarctica, Ann. Glaciol., 46, 29–34, 2007.

Picard, G., Brucker, L., Roy, A., Dupont, F., Fily, M., Royer, A., and Harlow, C.: Simulation of the microwave emission of multilayered snowpacks using the Dense Media Radiative transfer theory: the DMRT-ML model, Geosci. Model Dev., 6, 1061–1078, https://doi.org/10.5194/gmd-6-1061-2013, 2013.

Ridley, J.: Surface melting on Antarctic Peninsula ice shelves detected by passive microwave sensors, Geophys. Res. Lett., 20, 2639–2642, https://doi.org/10.1029/93GL02611, 1993.

Scambos, T. A., Hulbe, C., Fahnestock, M., and Bohlander, J.: The link between climate warming and break-up of ice shelves in the Antarctic Peninsula, J. Glaciol., 46, 516–530, https://doi.org/10.3189/172756500781833043, 2000.

Scott, R. C., Nicolas, J. P., Bromwich, D. H., Norris, J. R., and Lubin, D.: Meteorological drivers and large-scale climate forcing of West Antarctic surface melt, J. Climate, 32, 665–684, https://doi.org/10.1175/JCLI-D-18-0233.1, 2019.

Surdyk, S.: Using microwave brightness temperature to detect short-term surface air temperature changes in Antarctica: An analytical approach, Remote Sens. Environ., 80, 256–271, https://doi.org/10.1016/S0034-4257(01)00308-X, 2002.

Tedesco, M.: Snowmelt detection over the Greenland ice sheet from SSM/I brightness temperature daily variations, Geophys. Res. Lett., 34, L02504, https://doi.org/10.1029/2006GL028466, 2007.

Tedesco, M.: Assessment and development of snowmelt retrieval algorithms over Antarctica from K-band spaceborne brightness temperature (1979–2008), Remote Sens. Environ., 113, 979–997, https://doi.org/10.1016/j.rse.2009.01.009, 2009.

Tedesco, M., Abdalati, W., and Zwally, H.: Persistent surface snowmelt over Antarctica (1987–2006) from 19.35 GHz brightness temperatures, Geophys. Res. Lett., 34, L18504, https://doi.org/10.1029/2007GL031199, 2007.

Torinesi, O., Fily, M., and Genthon, C.: Variability and trends of the summer melt period of Antarctic ice margins since 1980 from microwave sensors, J. Climate, 16, 1047–1060, 2003.

Trusel, L. D., Frey, K. E., and Das, S. B.: Antarctic surface melting dynamics: Enhanced perspectives from radar scatterometer data, J. Geophys. Res.-Earth, 117, F02023, https://doi.org/10.1029/2011JF002126, 2012.

Tsang, L. and Kong, J. A.: Scattering of Electromagnetic Waves, vol. 3: Advanced Topics, Wiley Interscience, New York, USA, 2001.

von Storch, H. and Zwiers, F. W.: Statistical analysis in climate research, Cambridge University Press, Cambridge, UK, 2001.

Wiesenekker, J., Kuipers Munneke, P., Van den Broeke, M., and Smeets, C.: A Multidecadal Analysis of Föhn Winds over Larsen C Ice Shelf from a Combination of Observations and Modeling, Atmosphere, 9, 172, https://doi.org/10.3390/atmos9050172, 2018.

Zheng, L., Zhou, C., and Liang, Q.: Variations in Antarctic Peninsula snow liquid water during 1999–2017 revealed by merging radiometer, scatterometer and model estimations, Remote Sens. Environ., 232, 111219, https://doi.org/10.1016/j.rse.2019.111219, 2019.

Zwally, J. H. and Fiegles, S.: Extent and duration of Antarctic surface melting, J. Glaciol., 40, 463–475, https://doi.org/10.3189/S0022143000012338, 1994.